Research Article

Nano Research
2022, 15(4): 3548–3555

ISSN 1998-0124 CN 11-5974/O4
https://doi.org/10.1007/s12274-021-3891-0

Large scale synthesis of full-color emissive carbon dots from a single carbon source by a solvent-free method

Hui Ding[1], Xuan-Xuan Zhou[1], Zi-Hui Zhang[1], Yun-Peng Zhao[1] (✉), Ji-Shi Wei[2], and Huan-Ming Xiong[2] (✉)

[1] *Key Laboratory of Coal Processing and Efficient Utilization of Ministry of Education and College of Chemical Engineering, China University of Mining and Technology, Xuzhou 221116, China*
[2] *Department of Chemistry and Shanghai Key Laboratory of Molecular Catalysis and Innovative Materials, Fudan University, Shanghai 200433, China*

Received: 5 July 2021 / **Revised:** 11 September 2021 / **Accepted:** 15 September 2021

ABSTRACT

Full-color emissive carbon dots (CDs) hold a great promise for various applications, especially in light emitting diodes (LEDs). However, the existing synthetic routes for CDs are carried out in solutions, which suffer from low yields, high pressures, various byproducts, large amounts of waste solvents, and complicated photoluminescence (PL) origins. Therefore, it is necessary to explore large scale synthesis of CDs with high quantum yield (QY) across the entire visible range from a single carbon source by a solvent-free method. In this work, a series of CDs with tunable PL emission from 442 to 621 nm, QY of 23%–56%, and production yield within 34%–72%, are obtained by heating o-phenylenediamine with the catalysis of KCl. Detailed characterizations identify that, the differences between these CDs with respect to the graphitization degree, graphitic nitrogen content, and oxygen-containing functional groups, are responsible for their distinct optical properties, which can be modulated by controlling the deamination and dehydrogenation processes during reactions. Blue, green, yellow, red emissive films, and LEDs are prepared by dispersing the corresponding CDs into polyvinyl alcohol (PVA). All types of white LEDs (WLEDs) with high color-rendering-index (CRI), including warm WLEDs, standard WLEDs, and cool WLEDs, are also fabricated by mixing the red, green, and blue emissive CDs into PVA matrix by the appropriate ratios.

KEYWORDS

carbon dots, solvent-free synthesis, full-color luminescence, surface state, white light emitting diodes

1 Introduction

Full-color emissive carbon dots (CDs) are attracting great interests owning to their tunable photoluminescence (PL) emission under a single wavelength of excitation light and the resulting widespread applications [1–5]. Typically, the synthetic strategies for CDs are ascribed to two types, the top-down and the bottom-up [6–8]. The former includes chemically decomposing and electrochemically etching bulk carbon materials, while the latter involves thermal condensation and carbonization of small organic molecules or biomass. By far, the bottom-up strategy has been adopted by more and more researchers because it can choose from numerous carbon sources and various reaction conditions, and the resulting CDs possess better fluorescence properties, particularly the high quantum yields (QYs) in the long wavelength spectrum [9–11]. However, it requires a large amount of solvents as reaction mediums that may be expensive, flammable, or toxic, and the high pressure of solvents in enclosed reactors is always a danger for large scale production [12–16]. Many researchers have found that solvents could take part in reactions, so the purity and optical properties of the as-prepared CDs greatly depend on solvents, which render intricate growth processes and incomprehensible luminescence mechanisms [17–20]. In addition, the complicated mixture of products needs time-consuming post-treatment, leaving plenty of wastes and solvents that are difficult to handle [20–22]. Therefore, if CDs of high quality could be synthesized by a single carbon source in solvent-free reactions, the above problems would be resolved once and for all.

Although solvent-free syntheses of CDs from organics or biomass have been tried many years before, only a few researchers obtained highly fluorescent CDs [23]. And the solid state reactions produce much more aggregated large particles than mono-dispersed nanoparticles, so the production yields of CDs are always low [24]. Moreover, the degree of carbonization and graphitization of the obtained CDs is restricted owing to decreased pressure in reaction system, consequently resulting in their weak fluorescent intensity and low QY in the long wavelength region [25]. Recently, new strategies for the solvent-free synthesis of red emitting CDs with high PL QY and high production yield emerged, which decompose carbon sources within excess solid inorganic salts. For instance, through directly heating a mixture of o-phenylenediamine (o-PDA) and aluminum chloride hexahydrates ($AlCl_3·6H_2O$), Liu et al. prepared 57% efficient red emitting CDs with emission peak at 590 nm and production yield of 60% [13]. The introduced $AlCl_3·6H_2O$ was found to serve not only as dispersing medium to enhance production yield of CDs, but also as catalyst for enlarging efficient aromatic sp^2-conjugated system, which is favorable to red emission. This pioneer work implies that some inorganic salt could take part in the CD

Address correspondence to Yun-Peng Zhao, zhaoyp@cumt.edu.cn; Huan-Ming Xiong, hmxiong@fudan.edu.cn

formation to modulate the structural compositions and optical properties of CDs. Therefore, thermal treatment on a mixture of a carbon source and some organic salt is feasible for large scale syntheses of CDs with tunable PL and controlled structural compositions.

Herein, for the first time, we report a solid state synthesis of CDs with bright, stable, and full-color PL emission from a single carbon source of o-PDA, using KCl as a novel deamination and dehydrogenation catalyst. The production yields and absolute PL QYs of CDs reach up to 72% and 56%, respectively. The detailed characterizations prove that the energy gap and emission efficiency of CDs correlate with their graphitization degree and graphitic nitrogen contents, which can be readily tuned by controlling the deamination and dehydrogenation reactions between o-PDA molecules. Both PL mechanism and formation process of CDs are proposed on the basis of control experiments and detailed comparisons. These CDs are mixed with polyvinyl alcohol (PVA) matrix in appropriate ratios to fabricate full-color emissive films and monochromatic light-emitting diodes (LEDs), and even white LEDs (WLEDs) with high color-rendering-index (CRI), exhibiting immense potential for practical lighting applications.

2 Experimental

2.1 Materials

o-PDA, KCl, ethanol, and polyvinyl alcohol (M_W = 96,500) were purchased from Sinopharm Chemical Reagent Co., Ltd. (China). GaN LEDs chips without phosphor coating were purchased from Advanced Optoeletronic Technology CO., Ltd. All chemical reagents were analytical grade and used as received without any purification. Ultrapure (Milli-Q) water was used for all experiments.

2.2 Characterizations

The photographs were taken with a camera (Canon EOS 800D) under 365 nm ultraviolet (UV) light. Transmission electron microscope (TEM) and high-resolution TEM (HRTEM) images were obtained using a JEM-2010 TEM with an acceleration voltage of 200 kV. The ultraviolet–visible (UV–vis) absorption spectra were recorded on a Shimadzu UV-3101 PC spectrophotometer. The fluorescence spectra were registered at room temperature on a Horiba Jobin Yvon FluoroMax-4 spectrofluorometer. The Fourier-transform infrared (FTIR) spectra were recognized with a Nicolet Nexus 470 FTIR spectrometer. The Raman spectra were gathered using an XploRA Raman spectrometer at an excitation wavelength of 785 nm. The X-ray photoelectron spectra were measured with an AXIS Ultra DLD spectrometer. Time-resolved fluorospectroscopy was performed using an FLS 920 spectrometer. The photoelectric properties, including the emission spectra, correlated color temperature (CCT), CRI, and Commission Internationale de L' Eclairage (CIE) color coordinates of the WLEDs, were determined by using a high-accuracy array spectroradiometer (HAAS-2000, Everfine).

2.3 Syntheses of full-color emissive CDs

The tunable fluorescent CDs from blue to red were prepared by solvent-free carbonization treatment of o-PDA and KCl with different molar ratios under different reaction conditions. For blue emissive CDs, 25 mmol of o-PDA and 5 mmol of KCl were ground together in a mortar for 15 min. The mixture was then transferred into a 20 mL of Teflon-lined stainless-steel autoclave for heating 4 h at 180 °C. After the reaction, the obtained carbonized powder was washed with a mixture of ethanol and deionized water (volume ratio of 1:10) by three times to remove salt and impurities. The remnants were dispersed in ethanol and then centrifuged at 10,000 rpm for 6 min to remove the precipitate. The supernatant was collected and stored for further characterizations. For other CDs, their preparation processes were the same as the above except the reaction conditions. Specifically, the blue-green emissive CDs were obtained after 6 h reaction at 180 °C; the green emissive CDs were obtained after 8 h reaction at 180 °C; the yellow-green emissive CDs were obtained after 6 h reaction at 200 °C; the yellow emissive CDs were obtained after 8 h reaction at 200 °C; the red emissive CDs were obtained after 10 h reaction at 200 °C.

2.4 Preparation of full-color emissive films

For the blue/green/yellow/red florescent glass films, 1 mL of the corresponding CDs ethanol solution (10 mg·mL^{-1}) was mixed with 10 mL of PVA aqueous solution (0.20 g·mL^{-1}), and then dropped on a cleaned glass sheet followed by drying for 4 h under ambient circumstances.

2.5 Fabrication of LED devices

All types of WLEDs, including warm, standard, and cool WLEDs, were fabricated with a similar method but different weight ratios of B-CDs to G-CDs to R-CDs. For warm WLEDs, 0.4 mg of B-CDs, 1.3 mg of G-CDs, and 2.1 mg of R-CDs were mixed with 60 mL of PVA ethanol solution (0.20 g·mL^{-1}), and then the homogeneous mixture was casted on a UV LED chip (365 nm). The obtained device was cured in an oven at 40 °C for 1 h. For standard WLEDs and cool WLEDs, their weight ratios of B-CDs, G-CDs, and R-CDs were changed to 0.6:1.9:1.5 and 0.8:1.5:0.9, respectively.

3 Results and discussion

The synthesis of full-color emission CDs from blue to red, as shown in Fig. 1(a), was achieved by solvent-free carbonization of a mixture of o-PDA and KCl in appropriate ratios under different reaction conditions, followed by simple solvent washing and centrifugal separation. Herein, KCl plays a key role for the successful preparation of full-color emissive CDs because without KCl, o-PDA solely produces blue to yellow emissive CDs (Fig. S1 in the Electronic Supplementary Material (ESM)). The yield of this facile reaction is about 72%, which is promising for industrial production (Fig. S2 and Table S1 in the ESM). The as-obtained CDs ethanol solutions display a clear color appearance under daylight and bright fluorescence colors from blue to red under a UV light of 365 nm (Fig. 1(b)). The PL emission maxima of these CDs are observed at 442, 468, 513, 547, 565, and 621 nm, respectively, covering the whole visible light region (Fig. 1(c)). Four typical CDs samples exhibiting blue, green, yellow, and red fluorescence are selected for further characterizations, which are labeled as B-CDs, G-CDs, Y-CDs, and R-CDs, respectively.

The UV–vis absorption spectra of the four selected samples in Figs. 2(c)–2(f) show similar absorption in the UV region (between 200–300 nm), but different absorption at longer-wavelength region. In the UV region of each curve, a peak at 282 nm is observed, corresponding to the π–π* transitions of C=C and C=N bonds in carbon cores [26], which do not generate fluorescence typically. However, at the longer-wavelength region, the four samples exhibit distinct absorption maxima/bands at 318, 434, 516, and 589 nm, indicating that there exist different kinds of surface state transitions in these CDs [27–29]. Similar to other reported CDs with uniform optical properties, the four selected CDs display excitation-independent PL emissions, that is, the PL

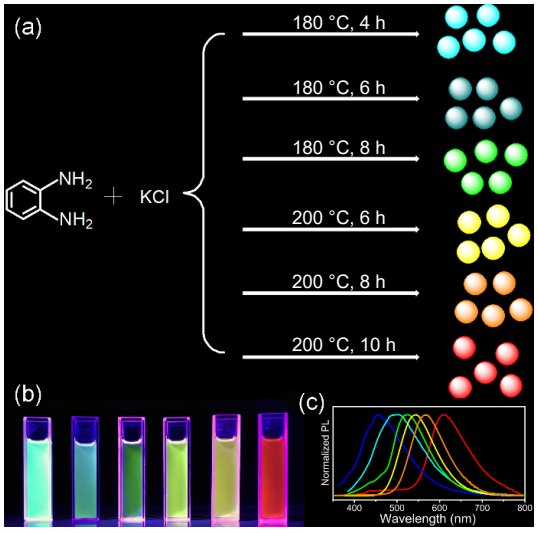

Figure 1 (a) A solvent-free reaction strategy to produce full-color fluorescent CDs from a single carbon source o-PDA with the catalysis of KCl. (b) Fluorescence images of the as-prepared CDs under 365 nm of UV light. (c) Normalized PL spectra of all the above CDs samples under 365 nm of UV light.

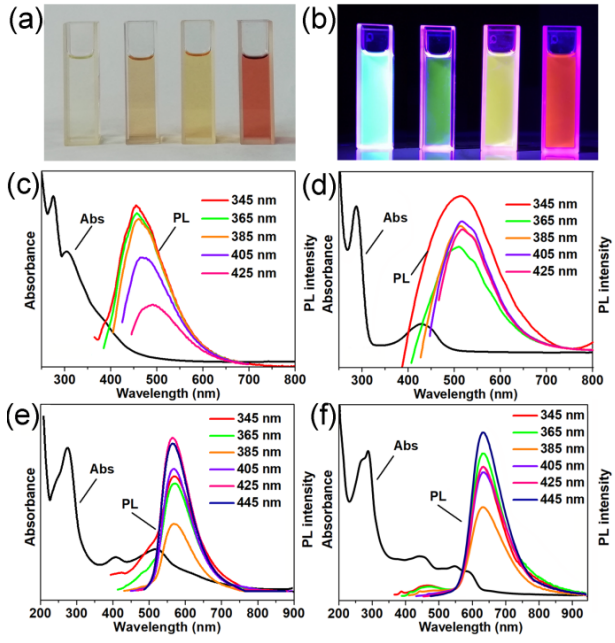

Figure 2 Optical photographs of the four selected CDs in ethanol under (a) daylight and (b) UV light, respectively. Absorption spectra and PL emission spectra of (c) B-CDs, (d) G-CDs, (e) Y-CDs, and (f) R-CDs under excitation with light of different wavelengths.

emission peaks of our samples keep constant when different excitation wavelengths are applied. The absolute QYs for B-, G-, Y-, and R-CDs are measured to be 56.2%, 23.4%, 41.7%, and 32.8%, respectively, using an integrating sphere under their optimal excitation wavelengths (Table S1 in the ESM). Moreover, the time-resolved PL decay spectra of these samples (Fig. S3 in the ESM) show that they can be fitted into two exponentials, a short-lived component τ_1 (about 0.5 ns) and a long-lived component τ_2 (about 5.5 ns), corresponding to the radiative recombination of the intrinsic states and the surface states, respectively [30–32]. The averaged lifetime for the samples from B-CDs to R-CDs increases from 3.93 to 5.38 ns (Table S2 in the ESM), as the τ_1 proportion increases from 12.24% to 24.64%, suggesting that the strong coupling exists between the surface states and the intrinsic states and that the core states in the radiative lifetime of these CDs play a positive role in determining their PL redshift [33]. In brief, the above data demonstrate that our CDs possess excellent uniform optical properties, and their tunable PL emission is closely related to their carbon cores, which can be modulated by controlling the reaction conditions under the assistance of KCl.

TEM images presented in Figs. 3(a)–3(d) exhibit that the four selected samples are well-dispersed and homogeneous nanodots with similar average sizes of about 2.6 nm (Figs. 3(i)–3(l)). The HRTEM images provided in the insets illustrate that all these four CDs have highly crystalline carbon structure with identical well-resolved lattice fringes. The lattice fringe distance is observed at 0.21 nm, corresponding to the (100) in-plane lattice of grapheme [34]. The atomic force microscope (AFM) images (Figs. 3(e) and 3(f)) show that these monodispersed CDs have a similar thickness of 4.0–5.5 nm, larger than the diameters observed by TEM, which is due to the existence of polymer chain shells [4]. The TEM and AFM data clearly demonstrate that the observed PL redshift in these CDs is not due to quantum size effects. The X-ray diffraction (XRD) patterns (Fig. S4 in the ESM) show a sharp peak at around 26.3° with enhanced intensity, signifying a gradually increasing degree of graphitization from B-CDs to R-CDs [35]. The Raman spectra of these samples, as shown in Fig. 4, reveal two peaks at 1,371 and 1,592 cm^{-1}, corresponding to the disordered structures or defects (D band) and the graphitic carbon domains (G band) of carbon materials, respectively [36]. The intensity ratio of I_D/I_G is 0.94, 0.89, 0.83, and 0.76 for B-, G-, Y-, and R-CDs, respectively, indicating a gradual increase in the size of sp^2-domains, which is in accordance with the above TEM and XRD results.

The compositions of the four samples are further analyzed by FTIR spectra and X-ray photoelectron spectroscopy (XPS). In Fig. 5, the FTIR spectra reveal that all these CDs contain many hydrophilic groups, such as O–H/N–H at 3,300 to 3,470 cm^{-1}, C=O at 1,680 cm^{-1}, and C–O at 1,124 cm^{-1} [37], thereby endowing these CDs with excellent solubility in polar solvents. Furthermore, the FTIR spectra show that as the observed PL redshifts from B-CDs to R-CDs, both the stretching vibration intensities of C=N at 1,585 cm^{-1} and C=C at 1,521 cm^{-1} gradually increase while the stretching vibration intensity of C=O at 1,682 cm^{-1} decreases significantly, reflecting a gradually increasing content of the nitrogen-containing poly-aromatic structures [38]. XPS measurements were also performed to characterize the surface groups of these samples. The full XPS spectra (Fig. S5 in the ESM) display three typical peaks at 285, 400, and 531 eV, corresponding to C 1s, N 1s, and O 1s, respectively, demonstrating that all the CDs have the same elemental compositions. In the high-resolution XPS spectra (Fig. 6), the C 1s band can be deconvoluted into four binding energy peaks, relevant to C=C/C–C (284.2 eV), C–N (285.3 eV), C–O (286.5 eV), and C=O (288.1 eV), respectively [39]. The N 1s spectra are decomposed into three peaks at 399.4, 400.3, and 401.4 eV, representing pyridinic N, amino N, and graphitic N, respectively [40]. The O 1s spectra display two peaks at 531.4 and 533.3 eV for C=O and C–O bands, respectively. These results show that, as the PL redshifts, the element content declines from 2.88% to 0.97% for O, and from 16.12% to 14.1% for N (Table S3 in the ESM), respectively, indicating an increasing degree of graphitization in these CDs through the deamination and dehydrogenation reactions between adjacent o-PDA molecules during heating treatment [36].

Meanwhile, the sp^2 carbon content gradually increases from 0.56 (B-CDs) to 0.60 (R-CDs) as the graphitic N content also increases from 0.08 (B-CDs) to 0.23 (R-CDs) (Tables S4 and S5 in the ESM), again suggesting an increase in the size of sp^2-conjugated domains in these CDs [41], which agrees well with their increased graphitization degrees and graphitic nitrogen contents. Obviously, the above data demonstrate that our CDs comprise carbon cores with large conjugated sp^2 domains coated with abundant oxygen/nitrogen-containing surface groups, and

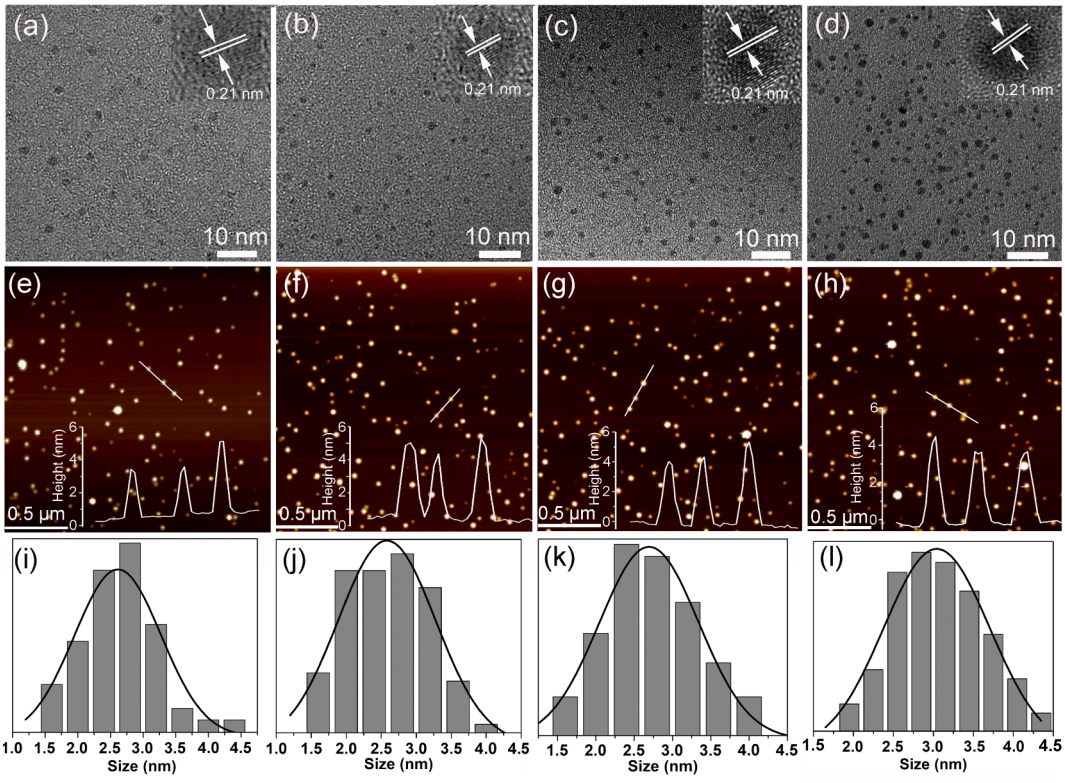

Figure 3 TEM and HRTEM images (inset) of (a) B-CDs, (b) G-CDs, (c) Y-CDs, and (d) R-CDs. AFM images of (e) B-CDs, (f) G-CDs, (g) Y-CDs, and (h) R-CDs. Particle size distribution diagrams of (i) B-CDs, (j) G-CDs, (k) Y-CDs, and (l) R-CDs. White lines are the height-profiles analysis along the corresponding lines in (e)–(h).

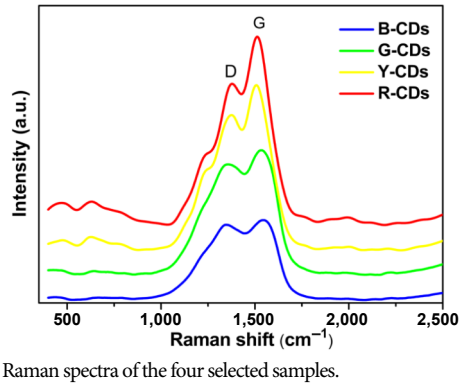

Figure 4 Raman spectra of the four selected samples.

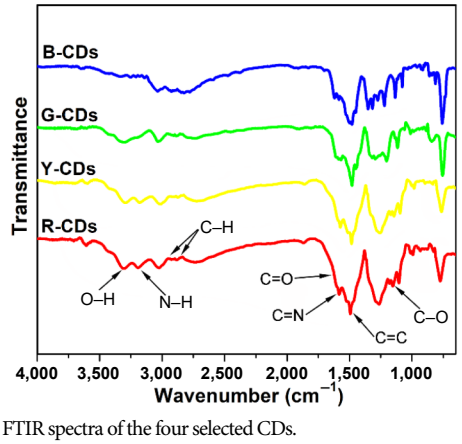

Figure 5 FTIR spectra of the four selected CDs.

that both their graphitization degree and graphitic nitrogen contents increase concurrently when their PL emissions shift from blue to red.

To study both the formation mechanism and the PL mechanism for these CDs, the influence of dosage of KCl on the microstructure and optical properties of CDs were investigated, in which the reaction conditions were kept the same as those of the R-CDs except for adding different amounts of KCl. Three kinds of CDs, namely CDs-2, CDs-4, and CDs-6, were specially produced by adding 2, 4, and 6 mmol of KCl, respectively. TEM images (Fig. S6 in the ESM) of the three CDs show their average sizes are near 2.5 nm, equivalent to those of R-CDs, but the carbonized degree of CDs increases gradually, indicating that the KCl catalyst has accelerated the deamination and dehydrogenation reactions between o-PDA without altering their particle sizes [27]. In Fig. S7 in the ESM, PL spectra of three kinds of CDs exhibit red-shifted emission peaks from 570 to 651 nm with KCl increment, confirming that KCl contributes to the observed PL redshift in CDs through improving their graphitization degree. Notably, although the CDs-6 sample has the highest degree of graphitization and the longest PL emission wavelength, its QY drops to 0.8%, which can be ascribed to the excessive carbonization of functional groups on CD surfaces [42]. Based on these results and those previous reports, a possible model is proposed for illustrating the formation mechanism of our CDs, as shown in Scheme 1(a). At the initial reaction stage, polymerization happens between the adjacent o-PDA molecules under high temperature and high pressure, which could be considered as a building block due to their smallest sp^2 domain with $-NH_2$ groups [43]. As the reaction temperature further increases, these intermediate crosslinking polymers are *in situ* carbonized together with deamination and dehydrogenation reactions [36], yielding conjugated sp^2 cluster with C=O, C–N, C=N, O–H, and N–H bonds. In the whole process, two points are important to the successful production of such CDs. One is that the core structures of CDs are modulated in a wide range through synergistically controlling the heating temperature and the heating durations with the catalyst KCl. The other is that KCl also plays as dispersing medium, thereby guaranteeing good dispersion of the obtained CDs [13]. In this way, the uniform and mono-dispersed CDs with high efficient full-color emission are produced on a large scale

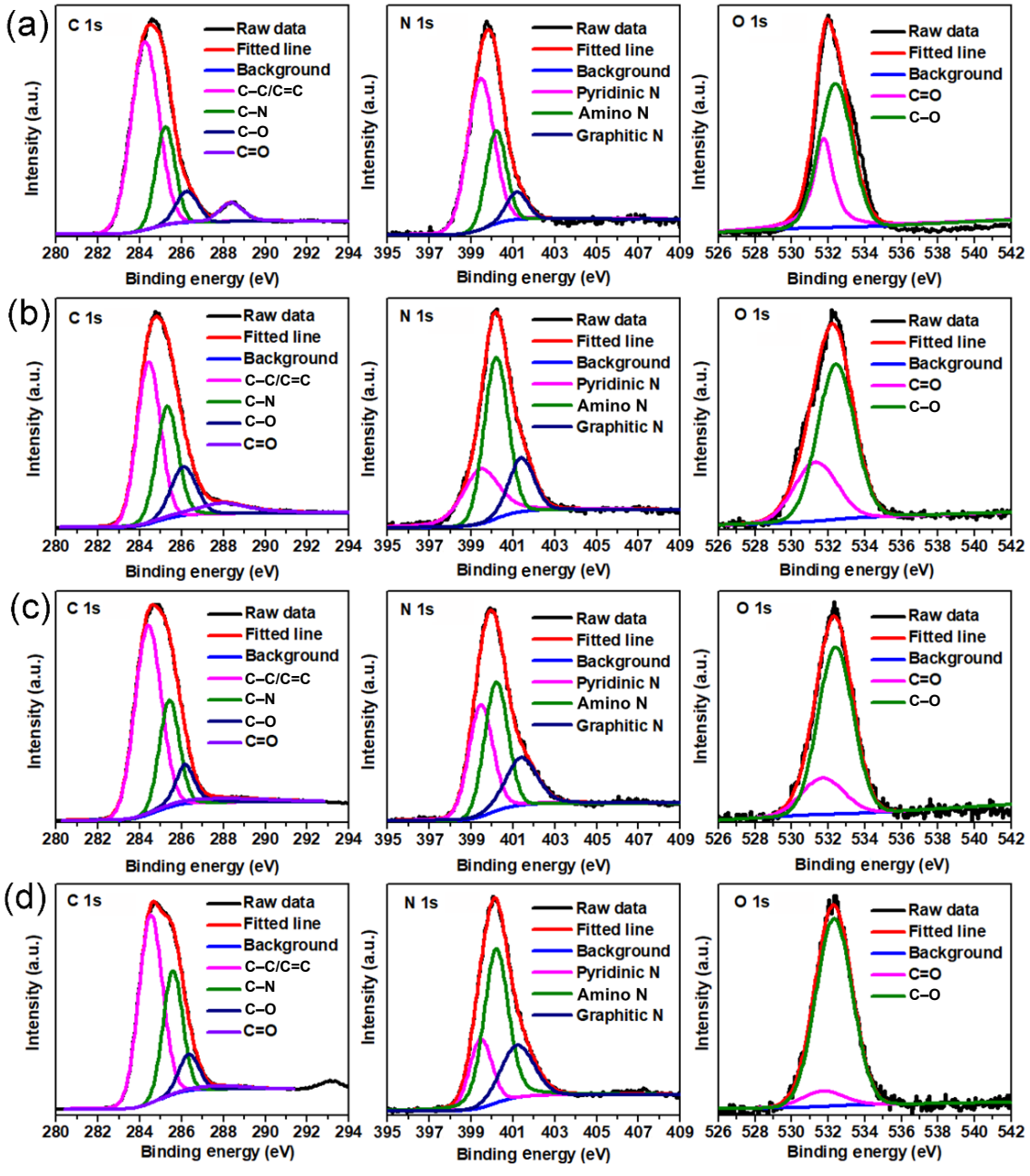

Figure 6 High-resolution XPS C 1s, N 1s, and O 1s spectra of the selected (a) B-CDs, (b) G-CDs, (c) Y-CDs, and (d) R-CDs, respectively.

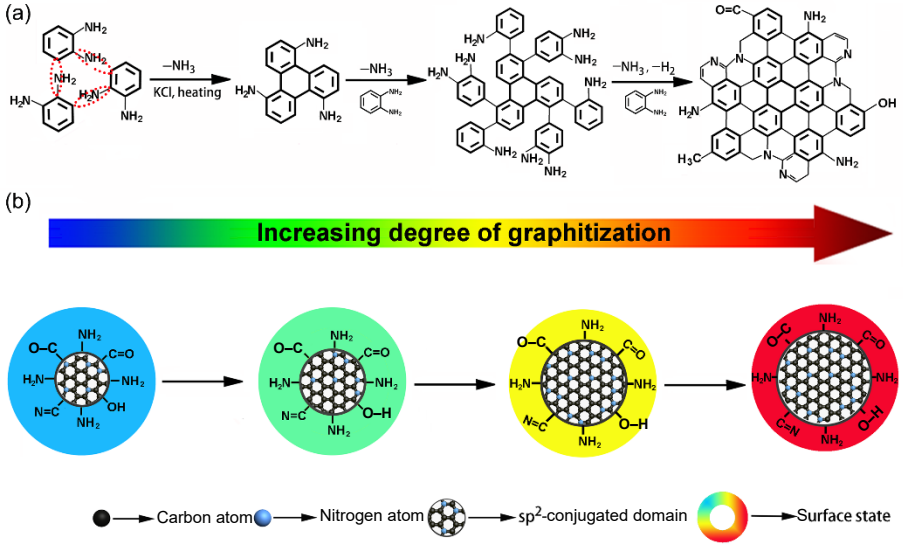

Scheme 1 A possible (a) formation mechanism and (b) PL mechanism for CDs with tunable PL emission.

finally.

To date, although the PL mechanisms of CDs remain a matter under debate, two popular models have been proposed for their PL redshift, including band-edge exciton emission and surface-defect state emission [10, 44]. In keeping with the former mechanism, several reports attributed the PL red shift of CDs to quantum size effect. However, in the present research, surface-defect states are regarded as dominate factor controlling the tunable PL emissions of our CDs because they have no obvious changes in particle size but evident pH-dependent PL emission (Fig. S8 in the ESM), which are similar to the observed performance of other reported CDs with a surface state controlled PL mechanism [26, 33]. Meanwhile, detailed structural and compositional analyses show that the tunable PL emission of CDs depends heavily on both the sp^2-conjugated domains and the graphitic nitrogen content. It has been reported that the surface-defect states of CDs are based on the synergistic hybridization of the carbon backbones and the connected functional groups, and the corresponding energy gap is highly associated with the extent of the π-electron conjugation and the graphitic nitrogen content [45]. When the π-electron system or graphitic nitrogen content improves within CD growth, smaller energy gaps of the surface states would form, thereby tuning the emission peak of CDs toward longer wavelength regions. Recently, the theoretical modeling and calculations based on density functional theory reported by Chen and coworkers also demonstrated that [46], as the graphitization extent or graphitic nitrogen content increases, narrowed band gaps between the highest occupied molecular orbital and the lowest unoccupied molecular orbital are created within the original gap of initial CDs, consequently leading to the pronounced fluorescence red shift. As a result, by modulating the deamination and dehydrogenation reactions between o-PDA, PL color of CDs can be tuned accordingly from blue to red across the entire visible spectrum (Scheme 1(b)).

Remarkably, due to the improved content of graphitic nitrogen atoms, the rigidity of the conjugated sp^2-domains within carbon cores could also been enhanced, which makes a significant contribution to the photoluminescence quantum yields (PLQYs) through reducing the non-radiative relaxation of molecular vibrations on CD surfaces [33]. Consequently, the PLQYs of these CDs exhibit an upward trend to some extents with their PL red shift, which is contrary to surface-state emission nature [47]. In brief, we believe that PL of the as-obtained CDs arises from surface states, and that the corresponding energy gaps are significantly determined by both the graphitization degree and the graphitic nitrogen content.

To explore practical applications of these CDs, multi-color emissive composite films were prepared by mixing CDs with PVA aqueous solution, and then drying at room temperature (Fig. S9 in the ESM). Under UV light of 365 nm, these films emit bright fluorescence emission with peaks at 443, 513, 565, and 621 nm, respectively, as shown in Fig. 7(a) and Fig. S10 in the ESM, in accordance with the emission maxima of the original CDs. Afterwards, full-color LEDs and white LEDs were fabricated by coating 365 nm chips with the PVA composites containing CDs in appropriate mass ratios. In Fig. S11 in the ESM, the

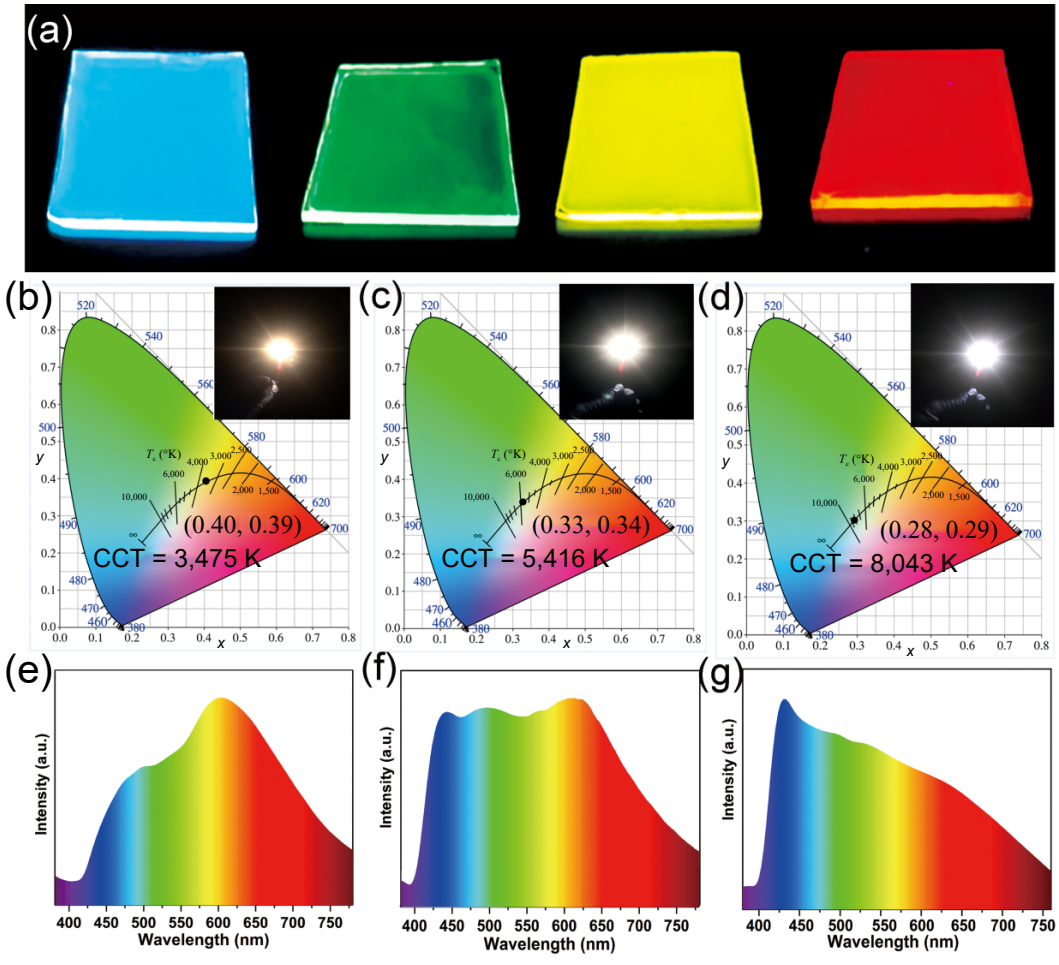

Figure 7 (a) Fluorescence images of CDs/PVA composite films on glass substrates under 365 nm of UV irradiation. From left to right, the samples are derived from B-CDs, G-CDs, Y-CDs and R-CDs, respectively. (b) The CIE color coordinates and (e) emission light spectrum of the warm WLED (inset: optical photograph of the warm WLED). (c) The CIE color coordinates and (f) emission light spectrum of the standard WLED (inset: optical photograph of the standard WLED). (d) The CIE color coordinates and (g) emission light spectrum of the cool WLED (inset: optical photograph of the cool WLED).

photographs of operating monochromatic down-conversion LEDs show that they are luminous with the CIE coordinates located at the vertices of a quadrangle, covering the entire visible spectrum (Fig. S12 in the ESM). The drive current-dependent PL spectra (Fig. S13 in the ESM) also reveal the good stability of these LEDs. In addition, by varying the ratios of B-CDs to G-CDs to R-CDs in PVA composites, all types of WLEDs could also be achieved, including warm-WLEDs, standard-WLEDs, and cool-WLEDs. Among them, the warm WLED with low correlated color temperature (CCT < 4,000 K) and high color rendering index (CRI > 80) is highly desired for indoor lighting because it makes our eyes relaxed and comfortable [48]. However, it remains difficult to make such a warm WLED because highly efficient red luminescent CD-based phosphors are rare. In our present research, a warm WLED fabricated with a weight ratio of 0.4:1.3:2.1 emits bright warm white light, with low correlated color temperature of 3,475 K, a CIE color coordinate of (0.40, 0.39) and a high-CRI of 90.1 (Fig. 7(b)). When the mass ratio is changed to 0.6:1.9:1.5, a standard WLED with a CIE color coordinate of (0.33, 0.34) is acquired (Fig. 7(c)), which is akin to natural sunlight [49]. The CCT of the standard WLED is 5,416 K and the CRI is as high as 86.4, even better than many previously reported CDs-based standard WLEDs. After changing the weight ratio to 0.8:1.5:0.9, a cool WLED with the CCT of 8,043 K, CIE coordinates of (0.28, 0.29), and CRI of 85.7 are obtained (Fig. 7(d)). The corresponding light-emitting spectra of all types of WLEDs, from Figs. 7(e)–7(g), cover the whole visible light region of 400–800 nm. Finally, the photo-stabilities of these WLEDs were tested (Fig. S14 in the ESM), and the results exhibit that their PL intensity remains unchanged after 7 days of continuous operation at 20 mA, demonstrating the excellent photostability of these WLED [50]. Overall, the full-color CDs-based phosphors are promising candidates for practical multicolor display and all types of high-CRI WLEDs applications.

4 Conclusions

In summary, distinguished from the conventional solution routes for CDs, we have successfully developed a facile, controllable, and solvent-free approach for large scale preparation of highly efficient full-color emissive CDs from a single carbon source. We found in the deamination and dehydrogenation processes, KCl plays a crucial role in manipulating the size of sp^2-conjugated domains and the content of graphitic nitrogen in CDs, so as to tune emission colors of CDs from blue to red. The resulting CDs possess a QY up to 56% and a yield up to 72%, and emit bright, stable, and tunable PL both in solution and in PVA matrixes under UV light. Various LEDs, including warm WLEDs, standard WLEDs, and cool WLEDs, have been fabricated by mixing one or more types of these CDs in appropriate ratios with the PVA colloids. The CIE color coordinates are precisely matched with the black body Planckian locus, and these WLEDs show high CRI above 80. Our present work provides a facile solvent-free method to produce CDs with high production yields and excellent optical properties, which is promising for the industrial production and the practical application.

Acknowledgements

This work was financially supported by the National Natural Science Foundation of China (Nos. 51803233, 21771039, and 21975048), and China Postdoctoral Science Foundation (No. 2019M651999).

Electronic Supplementary Material: Supplementary material (materials, experimental procedures, XRD patterns, and PL spectra) is available in the online version of this article at https://doi.org/10.1007/s12274-021-3891-0.

References

[1] Ding, H.; Zhou, X. X.; Wei, J. S.; Li, X. B.; Qin, B. T.; Chen, X. B.; Xiong, H. M. Carbon dots with red/near-infrared emissions and their intrinsic merits for biomedical applications. *Carbon* **2020**, *167*, 322–344.

[2] Liu, J. J.; Li, R.; Yang, B. Carbon dots: A new type of carbon-based nanomaterial with wide applications. *ACS Cent. Sci.* **2020**, *6*, 2179–2195.

[3] Nguyen, H. A.; Srivastava, I.; Pan, D.; Gruebele, M. Unraveling the fluorescence mechanism of carbon dots with *sub*-single-particle resolution. *ACS Nano* **2020**, *14*, 6127–6137.

[4] Liu, J. J.; Geng, Y. J.; Li, D. W.; Yao, H.; Huo, Z. P.; Li, Y. F.; Zhang, K.; Zhu, S. J.; Wei, H. T.; Xu, W. Q. et al. Deep red emissive carbonized polymer dots with unprecedented narrow full width at half maximum. *Adv. Mater.* **2020**, *32*, 1906641.

[5] Shi, X. X.; Meng, H. M.; Sun, Y. Q.; Qu, L. B.; Lin, Y. H.; Li, Z. H.; Du, D. Far-red to near-infrared carbon dots: Preparation and applications in biotechnology. *Small* **2019**, *15*, 1901507.

[6] Xia, C. L.; Zhu, S. J.; Feng, T. L.; Yang, M. X.; Yang, B. Evolution and synthesis of carbon dots: From carbon dots to carbonized polymer dots. *Adv. Sci.* **2019**, *6*, 1901316.

[7] Qu, D.; Sun, Z. C. The formation mechanism and fluorophores of carbon dots synthesized via a bottom-up route. *Mater. Chem. Front.* **2020**, *4*, 400–420.

[8] Zhu, Z. J.; Zhai, Y. L.; Li, Z. H.; Zhu, P. Y.; Mao, S.; Zhu, C. Z.; Du, D.; Belfiore, L. A.; Tang, J. G.; Lin, Y. H. Red carbon dots: Optical property regulations and applications. *Mater. Today* **2019**, *30*, 52–79.

[9] Gao, D.; Zhao, H.; Chen, X.; Fan, H. Recent advance in red-emissive carbon dots and their photoluminescent mechanisms. *Mater. Today Chem.* **2018**, *9*, 103–113.

[10] Liu, Y. H.; Huang, H.; Cao, W. J.; Mao, B. D.; Liu, Y.; Kang, Z. H. Advances in carbon dots: From the perspective of traditional quantum dots. *Mater. Chem. Front.* **2020**, *4*, 1586–1613.

[11] Xu, D.; Lin, Q. L.; Chang, H. T. Recent advances and sensing applications of carbon dots. *Small Methods* **2020**, *4*, 1900387.

[12] Liu, M. L.; Chen, B. B.; Li, C. M.; Huang, C. Z. Carbon dots: Synthesis, formation mechanism, fluorescence origin and sensing applications. *Green Chem.* **2019**, *21*, 449–471.

[13] Liu, K. K.; Song, S. Y.; Sui, L. Z.; Wu, S. X.; Jing, P. T.; Wang, R. Q.; Li, Q. Y.; Wu, G. R.; Zhang, Z. Z.; Yuan, K. J. et al. Efficient red/near-infrared-emissive carbon nanodots with multiphoton excited upconversion fluorescence. *Adv. Sci.* **2019**, *6*, 1900766.

[14] Wei, J. Y.; Lou, Q.; Zang, J. H.; Liu, Z. Y.; Ye, Y. L.; Shen, C. L.; Zhao, W. B.; Dong, L.; Shan, C. X. Scalable synthesis of green fluorescent carbon dot powders with unprecedented efficiency. *Adv. Opt. Mat.* **2020**, *8*, 1901938.

[15] Lu, S. Y.; Sui, L. Z.; Liu, J. J.; Zhu, S. J.; Chen, A. M.; Jin, M. X.; Yang, B. Near-infrared photoluminescent polymer-carbon nanodots with two-photon fluorescence. *Adv. Mater.* **2017**, *29*, 1603443.

[16] Zhu, Z. J.; Cheng, R.; Ling, L. T.; Li, Q.; Chen, S. Rapid and large-scale production of multi-fluorescence carbon dots by a magnetic hyperthermia method. *Angew. Chem., Int. Ed.* **2020**, *59*, 3099–3105.

[17] Soni, N.; Singh, S.; Sharma, S.; Batra, G.; Kaushik, K.; Rao, C.; Verma, N. C.; Mondal, B.; Yadav, A.; Nandi, C. K. Absorption and emission of light in red emissive carbon nanodots. *Chem. Sci.* **2021**, *12*, 3615–3626.

[18] Essner, J. B.; Kist, J. A.; Polo-Parada, L.; Baker, G. A. Artifacts and errors associated with the ubiquitous presence of fluorescent impurities in carbon nanodots. *Chem. Mater.* **2018**, *30*, 1878–1887.

[19] Wei, S. Q.; Yin, X. H.; Li, H. Y.; Du, X. Y.; Zhang, L. M.; Yang, Q.; Yang, R. Multi-color fluorescent carbon dots: Graphitized sp^2 conjugated domains and surface state energy level co-modulate band gap rather than size effects. *Chem.—Eur. J.* **2020**, *26*, 8129–8136.

[20] Liu, H. J.; Lv, X. T.; Li, C. W.; Qian, Y.; Wang, X. Y.; Hu, L.;

Wang, Y. C.; Lin, W. C.; Wang, H. Direct carbonization of organic solvents toward graphene quantum dots. *Nanoscale* **2020**, *12*, 10956–10963.
[21] Wang, L.; Li, W. T.; Yin, L. Q.; Liu, Y. J.; Guo, H. Z.; Lai, J. W.; Han, Y.; Li, G.; Li, M.; Zhang, J. H. et al. Full-color fluorescent carbon quantum dots. *Sci. Adv.* **2020**, *6*, eabb6772.
[22] Wang, B. Y.; Yu, J. K.; Sui, L. Z.; Zhu, S. J.; Tang, Z. Y.; Yang, B.; Lu, S. Y. Rational design of multi-color-emissive carbon dots in a single reaction system by hydrothermal. *Adv. Sci.* **2020**, *8*, 2001453.
[23] Li, F.; Yang, D. Y.; Xu, H. P. Non-metal-heteroatom-doped carbon dots: Synthesis and properties. *Chem.—Eur. J.* **2019**, *25*, 1165–1176.
[24] Dong, Y. Q.; Pang, H. C.; Yang, H. B.; Guo, C. X.; Shao, J. W.; Chi, Y. W.; Li, C. M.; Yu, T. Carbon-based dots Co-doped with nitrogen and sulfur for high quantum yield and excitation-independent emission. *Angew. Chem., Int. Ed.* **2013**, *52*, 7800–7804.
[25] Zhou, J.; Yang, Y.; Zhang, C. Y. A low-temperature solid-phase method to synthesize highly fluorescent carbon nitride dots with tunable emission. *Chem. Commun.* **2013**, *49*, 8605–8607.
[26] Ding, H.; Yu, S. B.; Wei, J. S.; Xiong, H. M. Full-color light-emitting carbon dots with a surface-state-controlled luminescence mechanism. *ACS Nano* **2016**, *10*, 484–491.
[27] Miao, X.; Qu, D.; Yang, D. X.; Nie, B.; Zhao, Y. K.; Fan, H. Y.; Sun, Z. C. Synthesis of carbon dots with multiple color emission by controlled graphitization and surface functionalization. *Adv. Mater.* **2018**, *30*, 1704740.
[28] Lyu, B. W.; Li, H. J.; Xue, F. F.; Sai, L. M.; Gui, B. J.; Qian, D. J.; Wang, X. Y.; Yang, J. H. Facile, gram-scale and eco-friendly synthesis of multi-color graphene quantum dots by thermal-driven advanced oxidation process. *Chem. Eng. J.* **2020**, *388*, 124285.
[29] Sun, M. H.; Liang, C.; Tian, Z.; Ushakova, E. V.; Li, D.; Xing, G. C.; Qu, S. N.; Rogach, A. L. Realization of the photostable intrinsic core emission from carbon dots through surface deoxidation by ultraviolet irradiation. *J. Phys. Chem. Lett.* **2019**, *10*, 3094–3100.
[30] He, P.; Shi, Y. X.; Meng, T.; Yuan, T.; Li, Y. C.; Li, X. H.; Zhang, Y.; Fan, L. Z.; Yang, S. H. Recent advances in white light-emitting diodes of carbon quantum dots. *Nanoscale* **2020**, *12*, 4826–4832.
[31] Zhang, Y. J.; Yuan, R. R.; He, M. L.; Hu, G. C.; Jiang, J. T.; Xu, T.; Zhou, L.; Chen, W.; Xiang, W. D.; Liang, X. J. Multicolour nitrogen-doped carbon dots: Tunable photoluminescence and sandwich fluorescent glass-based light-emitting diodes. *Nanoscale* **2017**, *9*, 17849–17858.
[32] Jing, P. T.; Han, D.; Li, D.; Zhou, D.; Shen, D. Z.; Xiao, G. J.; Zou, B.; Qu, S. N. Surface related intrinsic luminescence from carbon nanodots: Solvent dependent piezochromism. *Nanoscale Horiz.* **2019**, *4*, 175–181.
[33] Ding, H.; Wei, J. S.; Zhang, P.; Zhou, Z. Y.; Gao, Q. Y.; Xiong, H. M. Solvent-controlled synthesis of highly luminescent carbon dots with a wide color gamut and narrowed emission peak widths. *Small* **2018**, *14*, 1800612.
[34] Yan, F. Y.; Jiang, Y. X.; Sun, X. D.; Wei, J. F.; Chen, L.; Zhang, Y. Y. Multicolor carbon dots with concentration-tunable fluorescence and solvent-affected aggregation states for white light-emitting diodes. *Nano Res.* **2020**, *13*, 52–60.
[35] Anwar, S.; Ding, H. Z.; Xu, M. S.; Hu, X. L.; Li, Z. Z.; Wang, J. M.; Liu, L.; Jiang, L.; Wang, D.; Dong, C. et al. Recent advances in synthesis, optical properties, and biomedical applications of carbon dots. *ACS Appl. Bio Mater.* **2019**, *2*, 2317–2338.
[36] Jia, H. R.; Wang, Z. B.; Yuan, T.; Yuan, F. L.; Li, X. H.; Li, Y. C.; Tan, Z. A.; Fan, L. Z.; Yang, S. H. Electroluminescent warm white light-emitting diodes based on passivation enabled bright red bandgap emission carbon quantum dots. *Adv. Sci.* **2019**, *6*, 1900397.
[37] Li, H. X.; Su, D. D.; Gao, H.; Yan, X.; Kong, D. S.; Jin, R.; Liu, X. M.; Wang, C. G.; Lu, G. Y. Design of red emissive carbon dots: Robust performance for analytical applications in pesticide monitoring. *Anal. Chem.* **2020**, *92*, 3198–3205.
[38] Wang, B. Y.; Li, J.; Tang, Z. Y.; Yang, B.; Lu, S. Y. Near-infrared emissive carbon dots with 33. 96% emission in aqueous solution for cellular sensing and light-emitting diodes. *Sci. Bull.* **2019**, *64*, 1285–1292.
[39] Li, D.; Liang, C.; Ushakova, E. V.; Sun, M. H.; Huang, X. D.; Zhang, X. Y.; Jing, P. T.; Yoo, S. J.; Kim, J. G.; Liu, E. S. et al. Thermally activated upconversion near-infrared photoluminescence from carbon dots synthesized via microwave assisted exfoliation. *Small* **2019**, *15*, 1905050.
[40] Wang, P.; Liu, C.; Tang, W. Q.; Ren, S. X.; Chen, Z. J.; Guo, Y. R.; Rostamian, R.; Zhao, S. L.; Li, J.; Liu, S. X. et al. Molecular glue strategy: Large-scale conversion of clustering-induced emission luminogen to carbon dots. *ACS Appl. Mater. Interfaces* **2019**, *11*, 19301–19307.
[41] Tian, Z.; Zhang, X. T.; Li, D.; Zhou, D.; Jing, P. T.; Shen, D. Z.; Qu, S. N.; Zboril, R.; Rogach, A. L. Full-color inorganic carbon dot phosphors for white-light-emitting diodes. *Adv. Opt. Mat.* **2017**, *5*, 1700416.
[42] Zhu, S. J.; Meng, Q. N.; Wang, L.; Zhang, J. H.; Song, Y. B.; Jin, H.; Zhang, K.; Sun, H. C.; Wang, H. Y.; Yang, B. Highly photoluminescent carbon dots for multicolor patterning, sensors, and bioimaging. *Angew. Chem., Int. Ed.* **2013**, *52*, 3953–3957.
[43] Wang, Z. F.; Yuan, F. L.; Li, X. H.; Li, Y. C.; Zhong, H. Z.; Fan, L. Z.; Yang, S. H. 53% Efficient red emissive carbon quantum dots for high color rendering and stable warm white-light-emitting diodes. *Adv. Mater.* **2017**, *29*, 1702910.
[44] Li, Z. Y.; Wang, L.; Li, Y.; Feng, Y. Y.; Feng, W. Frontiers in carbon dots: Design, properties and applications. *Mater. Chem. Front.* **2019**, *3*, 2571–2601.
[45] Tao, S. Y.; Zhu, S. J.; Feng, T. L.; Xia, C. L.; Song, Y. B.; Yang, B. The polymeric characteristics and photoluminescence mechanism in polymer carbon dots: A review. *Mater. Today Chem.* **2017**, *6*, 13–25.
[46] Chen, S. W.; Ullah, N.; Wang, T. Q.; Zhang, R. Q. Tuning the optical properties of graphene quantum dots by selective oxidation: A theoretical perspective. *J. Mater. Chem. C* **2018**, *6*, 6875–6883.
[47] Bao, L.; Liu, C.; Zhang, Z. L.; Pang, D. W. Photoluminescence-tunable carbon nanodots: Surface-state energy-gap tuning. *Adv. Mater.* **2015**, *27*, 1663–1667.
[48] Zhang, X. Q.; Yang, H. Y.; Wan, Z. J.; Su, T.; Zhang, X. J.; Zhuang, J. L.; Lei, B. F.; Liu, Y. L.; Hu, C. F. Self-quenching-resistant red emissive carbon dots with high stability for warm white light-emitting diodes with a high color rendering index. *Adv. Opt. Mat.* **2020**, *8*, 2000251.
[49] Qu, D.; Yang, D. X.; Sun, Y. K.; Wang, X. Y.; Sun, Z. C. White emissive carbon dots actuated by the H-/J-aggregates and Forster resonance energy transfer. *J. Phys. Chem. Lett.* **2019**, *10*, 3849–3857.
[50] Yuan, T.; Meng, T.; He, P.; Shi, Y. X.; Li, Y. C.; Li, X. H.; Fan, L. Z.; Yang, S. H. Carbon quantum dots: An emerging material for optoelectronic applications. *J. Mater. Chem. C* **2019**, *7*, 6820–6835.